small structures
www.small-structures.com

A Self-Healing Chemistry-Enabled Organic Cathode for Sustainable and Stable Sodium-Ion Batteries

Jinghao Huang, Shi Li, Eric Youngsam Kim, Lei Cheng, Gui-Liang Xu, Khalil Amine, Chunsheng Wang,* and Chao Luo**

Sodium-on batteries (SIBs) are promising alternatives to lithium-ion batteries (LIBs) because of the low cost, abundance, and high sustainability of sodium resources. Analogous to LIBs, the high-capacity electrodes in SIBs always suffer from rapid capacity decay upon long-term cycling due to the particle pulverization induced by a large volume change. Circumventing particle pulverization plays a critical role in developing high-energy and long-life SIBs. Herein, tetrahydroxy-1,4-benzoquinone disodium salt (TBDS) that can self-heal the cracks by hydrogen bonding between hydroxyl group and carbonyl group is employed as a cathode for sustainable and stable SIBs. The self-healing TBDS exhibits long cycle life of 1000 cycles with a high rate capability up to 2 A g^{-1} due to the fast Na-ion diffusion reaction in the TBDS cathode. The intermolecular hydrogen bonding has been comprehensively characterized to understand the self-healing mechanism. The hydrogen bonding-enabled self-healing organic materials are promising for developing high-energy and long-cycle-life SIBs.

1. Introduction

Li-ion batteries (LIBs) dominate the energy storage markets for portable electronics and electric vehicles due to the high energy density and long cycle life. However, the commercial LIBs suffer from limited and unevenly distributed lithium resources in the earth crust, motivating researchers to exploit low-cost and high-sustainability alternatives to LIBs. Sodium-ion batteries (SIBs) are promising alternatives to LIBs because of the abundance and low cost of sodium sources and the comparable reaction potential to Li (–2.71 V for Na/Na$^+$ vs. −3.04 V for Li/Li$^+$).[1–3] To achieve high-energy batteries, high-capacity electrodes have to be used, inducing fast capacity decay due to the particle pulverization caused by a large volume change during sodiation/desodiation cycles. The particle pulverization in SIBs is much more severe than that in LIBs, due to the 1.4 times larger ion size of Na$^+$ than Li$^+$.[4–6] Almost all high-capacity organic and inorganic electrode materials in SIBs suffer from severe particle pulverization.[7–11] Among all antipulverization technologies, self-healing chemistry stands out as an ideal solution because of the spontaneous healing process without the assistance of external additives and energy.

Self-healing chemistry, which plays a critical role in curing the mechanical injury of living organisms, widely exists in biological systems to automatically heal the cracks and damages in the living body. It is enabled by a self-motivated process, which recovers the damages by living body itself without any external assistance. Inspired by the self-healing chemistry in biological systems, considerable research efforts have been devoted to mimicking the self-healing process in the other fields such as organic materials, polymers, and biomaterials.[12–16] The self-healing process maintains the structural integrity and prolong the lifetime of materials without external input of additives and energy. Recently, the self-healing

J. Huang, E. Y. Kim, C. Luo
Department of Chemistry and Biochemistry
George Mason University
Fairfax, VA 22030, USA
E-mail: cluo@gmu.edu

S. Li
Material Science Division
Argonne National Laboratory
Lemont, IL 60439, USA

L. Cheng
Chemical Sciences Division
Oak Ridge National Laboratory
Oak Ridge, TN 37831, USA

G.-L. Xu, K. Amine
Chemical Sciences and Engineering Division
Argonne National Laboratory
Lemont, IL 60439, USA
E-mail: xug@anl.gov

C. Wang
Department of Chemical and Biomolecular Engineering
University of Maryland
College Park, MD 20742, USA
E-mail: cswang@umd.edu

C. Luo
Quantum Science & Engineering Center
George Mason University
Fairfax, VA 22030, USA

The ORCID identification number(s) for the author(s) of this article can be found under https://doi.org/10.1002/sstr.202300211.

DOI: 10.1002/sstr.202300211

chemistry was applied in rechargeable batteries to heal the cracks of electrode materials during battery cycling.[17–20] For example, the silicon anode in LIBs suffers from 400% volume expansion during the lithiation process, which causes severe particle pulverization of the micro-sized silicon.[21,22] Though decreasing the particle size of silicon to nanoscale mitigates the particle pulverization, it remarkably enhances the cost and reduces the volumetric capacity of the silicon anode.[23–27] Alternatively, the self-healing binder based on the hydrogen bonding was used to combine the cracked micro-size Si together through the binder and maintain the structure integrity of the micro-sized Si anode.[28] To ensure that all the binders are well contacted to form a 3D network, a high content of binder is required, reducing the overall capacity of the electrodes. To reduce the binder content but still maintain the self-healing capability, we developed a polymer binder (sodium alginate) that can self-heal the organic electrode material (sodium rhodizonate).[29] The oxygen-rich active material and hydroxyl group-rich polymer binder enable the self-healing chemistry in the organic electrode due to the hydrogen bonding between oxygen and hydroxyl group. To maintain the high self-healing capability, the amount of inactive polymer binder required in electrodes is higher than traditional electrodes. Moreover, the polymer binder can only bond with the surface of the organic micro-particles, but the cracks and pulverization in the organic micro-particles still exist and cannot be healed. In addition, the electrolyte will penetrate into cracks and form solid electrolyte interphase (SEI), reducing the ionic and electronic conductivity of Si electrodes. To suppress the formation of cracks, the active materials should have a capability to self-heal themselves, which is an ultimate solution for high-capacity electrodes. The active materials should have hydrogen bonds that can heal the cracks by these intermolecular hydrogen bonding and retains the mechanical and electronic properties of the materials upon long-term cycling.

Organic electrode materials have high molecular composition tunability and abundant structural diversity.[30–39] Hydrogen bonding has been demonstrated as an effective strategy to enhance the performance of organic electrode materials in alkali-ion batteries.[40–42] The organic materials that have hydrogen bonding can self-heal themselves through intermolecular hydrogen bonding without the assistance of external binder or other additives. In this work, an organic cathode material, tetrahydroxy-1,4-benzoquinone disodium salt (TBDS, **Figure 1**c), was selected as a model to demonstrate the concept of self-healing electrodes in SIBs because of the intermolecular hydrogen bonding between hydroxyl groups and carbonyl groups (Figure 1d). 2,5-Dihydroxy-1,4-benzoquinone (DHBQ, Figure 1a) and 2,5-dihydroxy-1,4-benzoquinone disodium salt (DBDS, Figure 1b) are employed as control electrodes. DHBQ without the sodium oxide groups suffers from fast capacity loss because of high solubility in the organic electrolyte, while DBDS without the hydroxyl groups cannot form the intermolecular hydrogen bonding to trigger self-healing chemistry in the organic cathode. The improved electrochemical performance of TBDS is due to the synergy of salinization and hydrogen bonding-enabled self-healing chemistry, which address the dissolution challenge and particle pulverization challenge of organic electrodes, respectively. Therefore, TBDS shows the best cycle life among the three organic materials. It delivers a high reversible capacity of

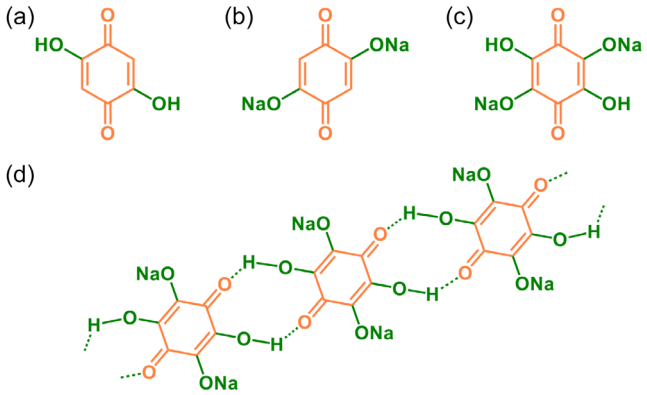

Figure 1. The molecular structure of a) DHBQ, b) DBDS, and c) TBDS; d) the schematic illustration for the intermolecular hydrogen bonding between TBDS molecules.

248.9 mAh g^{-1} at the current density of 20 mA g^{-1} and retains a reversible capacity of 107.5 and 76.6 mAh g^{-1} at the high current density of 1000 and 2000 mA g^{-1} for 1000 cycles, respectively. The isomer of TBDS with the same name (TBDS, $C_6H_2Na_2O_6$,) but different property also exhibited excellent performance in SIBs.[43] The superior electrochemical performance of TBDS demonstrates that the intermolecular hydrogen bonding-enabled self-healing chemistry is promising for high-stability and high-sustainability organic SIBs.

2. Results and Discussions

The self-healing organic material (TBDS) and control materials (DHBQ and DBDS) were characterized by X-ray diffraction (XRD), Raman spectroscopy, Fourier-transform infrared spectroscopy (FTIR), thermogravimetric analysis (TGA), scanning electron microscopy (SEM), and transmission electron microscopy (TEM). As shown in **Figure 2**a, S1a and S2a, Supporting Information, TBDS, DHBQ, and DBDS show sharp XRD peaks in the range from 10 degree to 80 degree, indicating good crystalline structures. In the Raman spectra (Figure 2b and S2b, Supporting Information), the sharp peak at ≈150 cm^{-1} represents the sodium-oxygen vibration, while the sharp peaks at ≈1550 cm^{-1} (Figure 2b), ≈1630 cm^{-1} (Figure S1b, Supporting Information), and ≈1600 cm^{-1} (Figure S2b, Supporting Information) represent the stretching vibration of carbonyl groups. The peak intensity of carbonyl groups is stronger in FTIR spectra than that in Raman spectra, so FTIR is a better technique to characterize the hydrogen bonding between hydroxyl group and carbonyl group. In the FTIR spectrum of TBDS (Figure 2c), the strong and broad peaks centered at ≈1480 cm^{-1} represent carbonyl groups, which also exist in DBDS (Figure S2c, Supporting Information) as a sharp peak at ≈1520 cm^{-1}. The redshift and broadening of the carbonyl peak for TBDS are owing to the hydrogen bonding, which lowers the energy of the carbonyl group. A good indication of the hydroxyl groups in TBDS is the broad shoulder from 3000 to 4000 cm^{-1} in Figure 2c, while only a weak peak at 2950 cm^{-1} is observed in Figure S2c, Supporting Information, coming from the C–H

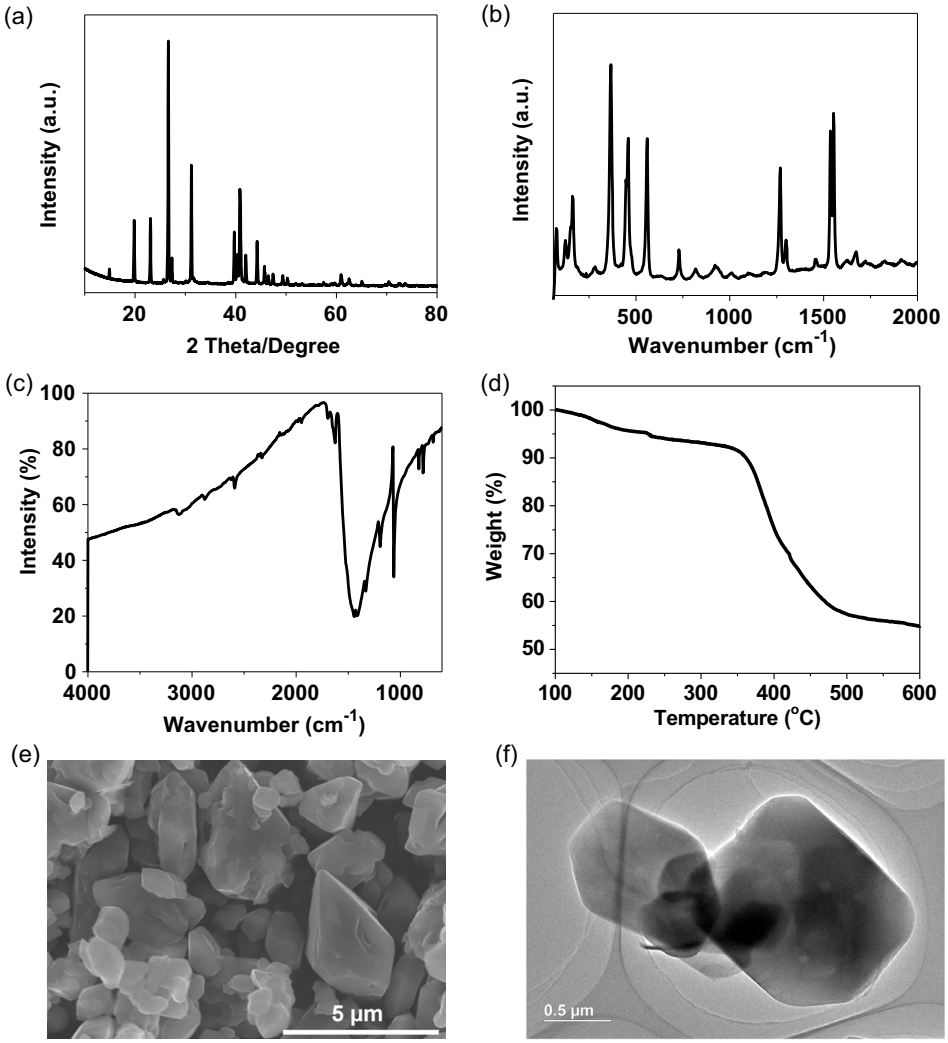

Figure 2. Material characterizations for TBDS. a) XRD pattern; b) Raman spectrum; c) FTIR spectrum; d) TG analysis; e) SEM image; f) TEM image.

stretching vibration in DBDS. Typically, hydroxyl group results in a sharp peak at ≈3700 cm^{-1}, but the formation of hydrogen bonding shifts the stretching vibration peak to lower frequencies by hundreds of wave numbers and flattened to give a broad band, which is also confirmed by the sharp peak at 3295 cm^{-1} for hydroxyl group in DHBQ (Figure S1c, Supporting Information).[44] The thermal stability of TBDS, DHBQ, and DBDS was studied by TGA. TBDS is stable up to 350 °C (Figure 2d), while DHBQ (Figure S1d, Supporting Information) and DBDS (Figure S2d, Supporting Information) are stable up to 150 and 450 °C, respectively. The slight weight loss from 100 to 200 °C in all three materials is due to the loss of water molecules from organic materials. The morphology of TBDS, DHBQ, and DBDS was characterized by SEM. As shown in Figure 2e, S1e and S2e, Supporting Information, TBDS and DBDS consist of micro-sized particles with a size about 1–5 μm, while DHBQ contains larger particles with a size about 10–100 μm. The shape and size of TBDS were further studied by TEM (Figure 2f), confirming the micro-sized structure. To further confirm the structure of the as-synthesized DBDS, we also performed nuclear magnetic resonance (NMR) spectroscopy and mass spectroscopy (MS) tests. The results are shown in Figure S3 and S4, Supporting Information. In the ^{1}H NMR spectrum (Figure S3a, Supporting Information), the peak at 4.85 ppm comes from the solvent, D_2O, and there are only one peak at 6.87 ppm from protons of DBDS. Since the two protons in DBDS are in the same chemical environment, there are only one type of proton in DBDS, which matches with the ^{1}H NMR result. Similarly, the three peaks in ^{13}C NMR spectrum (Figure S3b, Supporting Information) also agree with the three different types of carbons in DBDS. Furthermore, the MS result (Figure S4, Supporting Information) of 183.0 also matches with molar mass of DBDS, demonstrating that DBDS was successfully synthesized. The material characterizations prove the crystal and chemical structures, thermal stability, and micro-sized structure of TBDS, DHBQ, and DBDS. To study the self-healing chemistry of TBDS, electrochemical and in situ/ex situ characterizations were carried out.

The electrochemical behaviors of the self-healing material, TBDS, and control electrodes, DHBQ and DBDS, were evaluated

by galvanostatic charge and discharge. Though they show similar molecular structure, their redox plateaus are distinct. As shown in **Figure 3**a, S5a and S5c, Supporting Information, TBDS exhibits multiredox potentials in the range from 1.7 to 2.7 V, and DHBQ shows a pair of redox plateaus centered at 2.8 V, which are higher than that of DBDS in the potential range from 1.0 to 1.8 V. The increased reaction potential is due to the two hydroxyl groups, which change the electronic structure and molecular orbital energy levels of the organic compound. A cutoff window from 1.5 to 3.0 V was used for the test of TBDS to avoid the formation of SEI, which may prohibit the self-healing chemistry. The cyclic voltammogram of TBDS in Figure 3b further confirms the multiredox potentials in the range from 1.7 to 2.7 V, which are consistent with the galvanostatic charge and discharge curves. To further exploit the electrochemical performance, TBDS, DHBQ, and DBDS are tested at a low current density of 50 mA g^{-1}. TBDS exhibits a good cycling stability and retains a reversible capacity of ≈190 mAh g^{-1} after 100 cycles (Figure 3c), while DHBQ suffers from fast capacity decay due to the high solubility in the electrolyte (Figure S5b, Supporting Information), and DBDS shows an increased capacity in the initial 40 cycles and then suffers from capacity loss afterward (Figure S5d, Supporting Information). The Coulombic efficiency of both TBDS and DBDS is close to 100% upon long-term cycling. To prove that fast capacity loss of DHBQ is caused by its solubility in the electrolyte solvent (DEGDME), we performed a dissolution test. Two tubes were filled with the same amount of DEGDME, and ≈1 mg of DHBQ was added into one tube. After a while, the DHBQ solid was fully dissolved in DEGDME (Figure S6a, Supporting Information), and the color of the solution turns to yellow. Then, we performed the UV–Vis spectroscopy to further confirm the dissolution of DHBQ. As shown in Figure S6b, Supporting Information, compared with pure DEGDME, there is a sharp

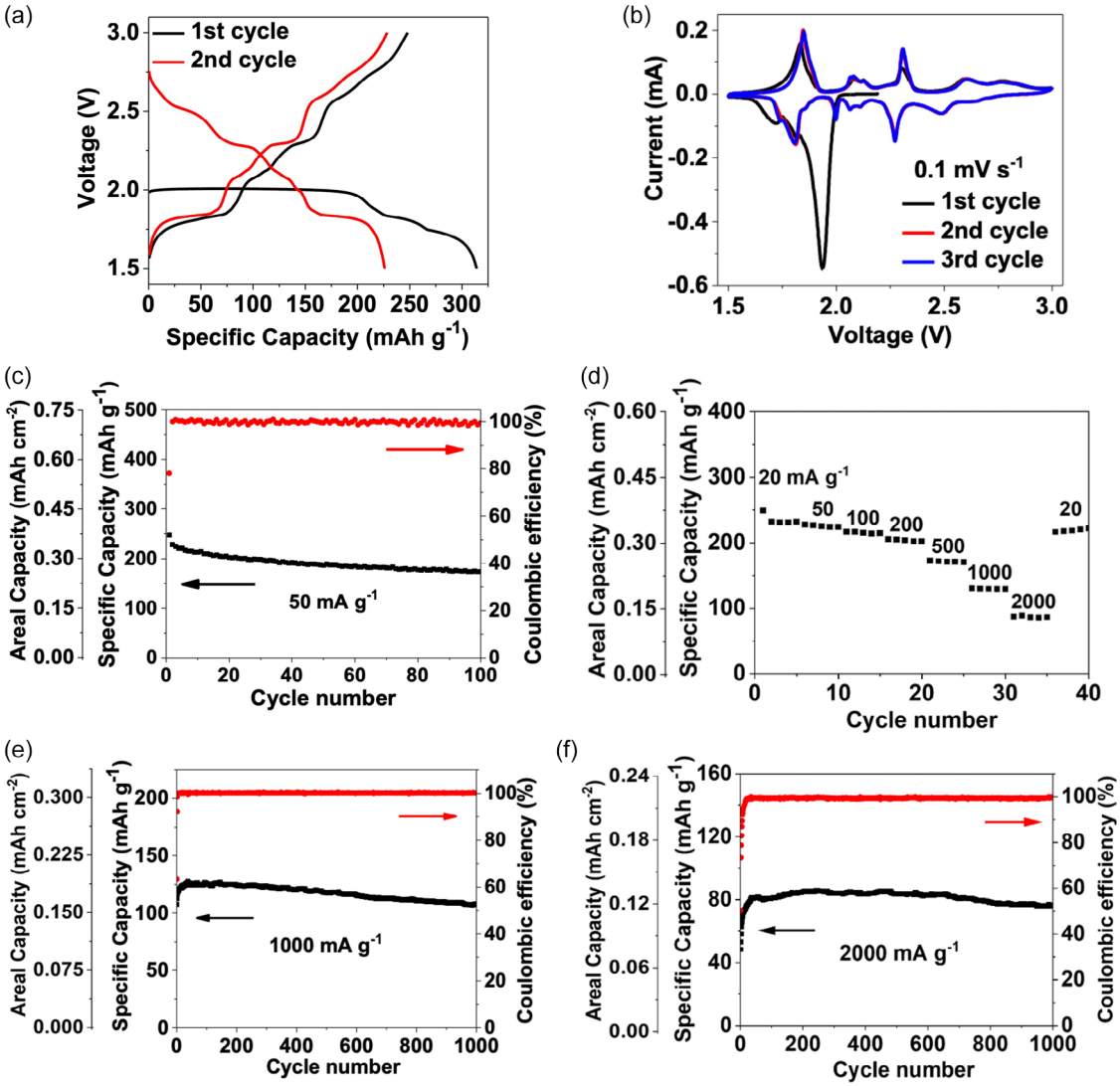

Figure 3. Electrochemical behaviors of TBDS in sodium-ion batteries. a) Galvanostatic charge and discharge curves at 50 mA g^{-1}; b) cyclic voltammograms; c) cycle life with Coulombic efficiency at 50 mA g^{-1}; d) rate capability at various current densities; e) cycle life with Coulombic efficiency at 1000 mA g^{-1}; f) cycle life with Coulombic efficiency at 2000 mA g^{-1}.

absorbance peak for the solution of DHBQ in DEGDME, which further indicates its dissolution in DEGDME. Therefore, the DHBQ molecules dissolve in the DEGDME electrolyte and then diffuse from the DHBQ electrode to the counter electrode. Chemical reactions, instead of electrochemical reactions, take place in the counter electrode, resulting in fast capacity loss of DHBQ in SIBs. Due to the stable cycle life of TBDS, we further explore its rate capability at various current densities from 20 to 2000 mA g^{-1}. The initial capacity of TBDS at 20 mA g^{-1} is 248.9 mAh g^{-1}, and it retains at 87.4 mAh g^{-1} even when the current density increases to 2000 mA g^{-1} (Figure 3d), demonstrating robust reaction kinetics. In comparison, we also tested the rate capability of DBDS from 20 to 2000 mA g^{-1}, and the result is shown in Figure S7, Supporting Information. DBDS shows an initial capacity of 140.0 mAh g^{-1} at 20 mA g^{-1} and retains a reversible capacity of 38.2 mAh g^{-1} at 2000 mA g^{-1}. The obvious difference of rate performances indicates faster reaction kinetics of TBDS. The long-term cyclic stability of TBDS is further studied at high current densities of 1 A g^{-1} and 2 A g^{-1}. As shown in Figure 3e,f, exceptional cyclic stability of 1000 cycles can still be achieved with negligible capacity loss, demonstrating excellent cycle life of the self-healing material.

The mechanism for fast reaction kinetics of TBDS is further investigated by cyclic voltammetry (CV) at various scan rates, galvanostatic intermittent titration technique (GITT), and electrochemical impedance spectroscopy (EIS). With elevated scan rates from 0.1 mV s^{-1} to 1.0 mV s^{-1} in CV (**Figure 4**a), the redox peak current remarkably enhances and the cathodic peak shifts to a lower potential, while the anodic peak shifts to a higher potential due to the increased polarization. The linear fit of natural logarithm relationship of scan rate and peak current in Figure 4b displays that the slopes of cathodic and anodic peaks are 0.607 and 0.539, respectively. Since the slope values are close to 0.5, the reaction kinetics of TBDS is mainly controlled by the Na-ion diffusion.[45] GITT is conducted to further study the overpotential and equilibrium potential of TBDS during initial charge and discharge cycles. As shown in Figure 4c–e, after one activation cycles, the sodiation/desodiation potentials in the second and

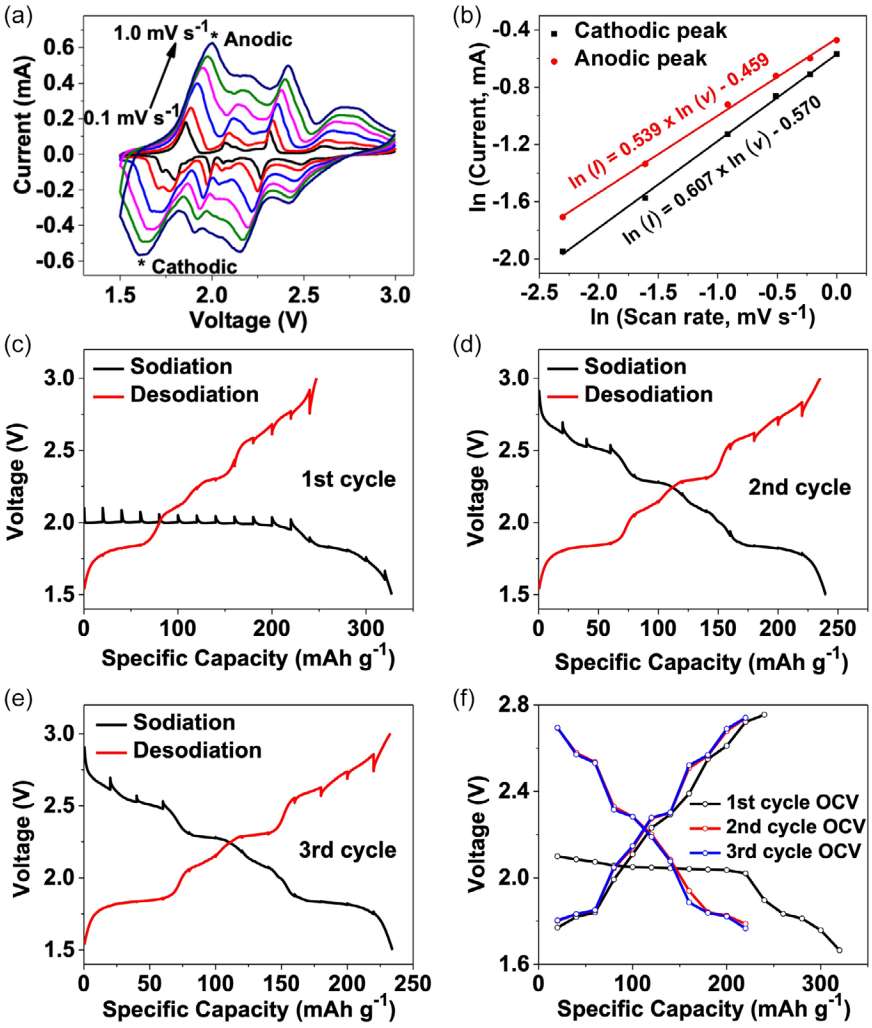

Figure 4. Reaction kinetics of TBDS. a) CV at various scan rates; b) the ln relationship of peak current and scan rate; potential response of TBDS electrode in the c) first cycle, d) second cycle, and e) third cycle during GITT measurements; f) equilibrium potential versus specific capacity during GITT measurement OCV = open-circuit potential.

third cycles show highly reversible multistep plateaus with very low overpotential, indicating a fast phase transition. The single flat potential plateau at 2.0 V with a high overpotential of ≈0.1 V in the first sodiation (Figure 4c) is due to the high stress and irreversible phase changes in the first lithiation process. To further explore reaction kinetics of the self-healing material (TBDS), EIS technique was conducted to understand the impedance evolution upon long-term cycling. The impedance spectra in Figure S8, Supporting Information show depressed semi-circles with slope tails where the semi-circle at a high-frequency region represents the interphase resistance of the TBDS electrode, while the straight line at the low-frequency region represents the diffusion resistance. During 50 cycles, the interphase resistance gradually increases from 5 Ohms to 35 Ohms. The small interphase resistance indicates fast reaction kinetics, which is consistent with the good capacity retention of TBDS at high current densities. The galvanostatic charge and discharge results prove that TBDS has higher cycling stability than DHBQ and DBDS, while the rate performance, CV, GITT, and impedance tests further confirm fast reaction kinetics of TBDS. The electrochemical results suggest that organic materials with self-healing hydrogen bonding are promising for SIBs. To understand the self-healing mechanism, we did theoretical calculations for DHBQ, DBDS, and TBDS molecules and in situ/ex situ characterizations for the pristine and cycled TBDS electrodes.

The IR spectroscopy for three materials was calculated at the B3LYP/6-311++G(d, p) level of theory, and the results are presented in Figure S9, Supporting Information. The stretching vibration of the carbonyl group in these materials was observed at 1736.13, 1684.21, and 1575.35 cm^{-1} for DHBQ, DBDS, and TBDS, respectively. The calculated carbonyl group frequencies generally follow the trend of experimental measurements. Next, we investigated the influence of hydrogen bonding on the IR peak shifts by studying the interaction between TBDS molecules. Specifically, we analyzed the potential energy surface as a function of the center of mass (COM) distance between two TBDS molecules, as depicted in Figure S10a, Supporting Information. The minimum energy configuration was found at a COM distance of 7.3 Å. The IR spectra of each TBDS dimer, as well as the TBDS monomer, were compared and shown in Figure S10b, Supporting Information. Notably, upon dimer formation through hydrogen bonding, the carbonyl peak of the TBDS monomer at 1564.92 cm^{-1} experiences a redshift to 1555.53 cm^{-1} when the COM distance is 7.3 Å. Moreover, the hydroxyl group in TBDS also exhibits lower frequencies and shows sensitivity to the COM distance between two TBDS dimers. This leads to the obvious peak shift in the IR spectra between 2200 and 3000 cm^{-1}, consistent with the observed broad shoulder in the experiment.

The intermolecular hydrogen bonding interactions among TBDS molecules were also investigated using molecular dynamics (MD) simulations. A simulation system consisting of 100 TBDS molecules and 240 ethanol molecules was placed in a cubic box. The system was then thermally equilibrated at a temperature of 300 K and 1 bar for a duration of 10 nanoseconds (ns). The radius distribution function (RDF) between the hydrogen (hydroxyl group) and oxygen (carbonyl group) was computed and is presented in Figure S11, Supporting Information.

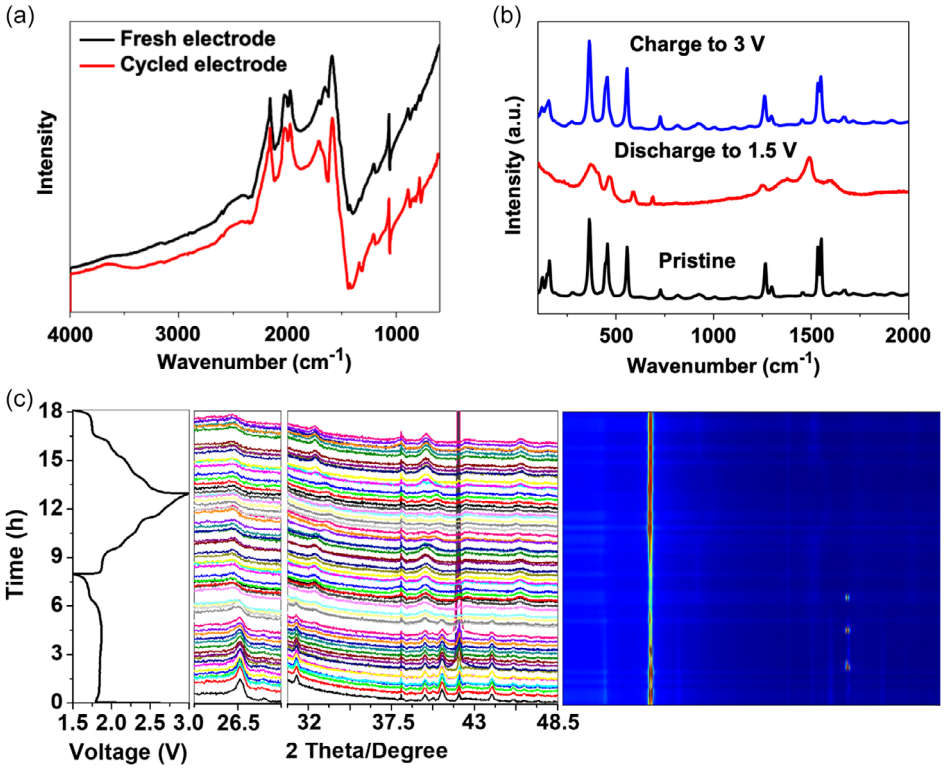

Figure 5. a) FTIR spectra of TBDS electrodes before and after cycling; b) Raman spectra of TBDS electrodes before and after cycling; c) in situ synchrotron XRD patterns and color-mapped profile of TBDS electrode and the corresponding voltage profile.

The presence of prominent peaks at 2.0 Å in the RDF indicates the formation of hydrogen bonds between adjacent TBDS molecules. Further analysis of the MD trajectory revealed the clusters of interconnected TBDS molecules through hydrogen bonding, as shown in Figure S11b, Supporting Information. Overall, our results offer computational insights into the presence of hydrogen bonds in the TBDS systems. The observed shift in the IR spectra is indicative of the significant influence of hydrogen bonding on the vibrational properties of the system. Furthermore, the calculated RDF and identification of hydrogen-bonded clusters in the MD trajectories reinforce the validity of the computational predictions, highlighting the importance of hydrogen bonding in governing the system's structural stability and dynamics. These findings contribute to an enhanced comprehension of the system's vibrational and structural properties.

To prove our hypothesis that the hydrogen bonding-induced self-healing chemistry alleviates particle pulverization in TBDS, ex situ FTIR, Raman spectroscopy, and in situ XRD characterizations were performed to study the structure and morphology evolution upon battery cycling. FTIR characterization of fresh and cycled TBDS electrodes shows similar absorption peaks in **Figure 5**a, indicating the structure of TBDS does not change before and after battery test. Analogous to FTIR results, Raman spectra in Figure 5b also exhibit the same Raman peaks in the spectra for the pristine TBDS electrode and cycled TBDS electrode at 3 V, confirming the good molecular structure retention of TBDS. When discharged to 1.5 V, the sharp Raman peak at $\approx$1550 cm^{-1} shifts to a lower value and becomes broad because of the redox reaction between oxygen in carbonyl groups and sodium ions, which lowers the vibration energy of the carbonyl group. After charged back to 3.0 V, all the peaks are recovered, demonstrating good molecular structure reversibility in SIBs. In addition to the molecular structure, we also investigated the crystal structure change of TBDS upon cycling. The in situ XRD results in Figure 5c display the crystal structure change during the initial charge and discharge. The XRD peaks at 26.5°, 31°, and 44° disappear after first discharge, while the other peaks from 35° to 43° retain after cycling. Several new peaks at 26°, 32.5°, and 46° appear after cycling, suggesting the crystal structure change after battery test. To further confirm it, ex situ XRD patterns for pristine and cycled TBDS electrodes after 1, 2 and

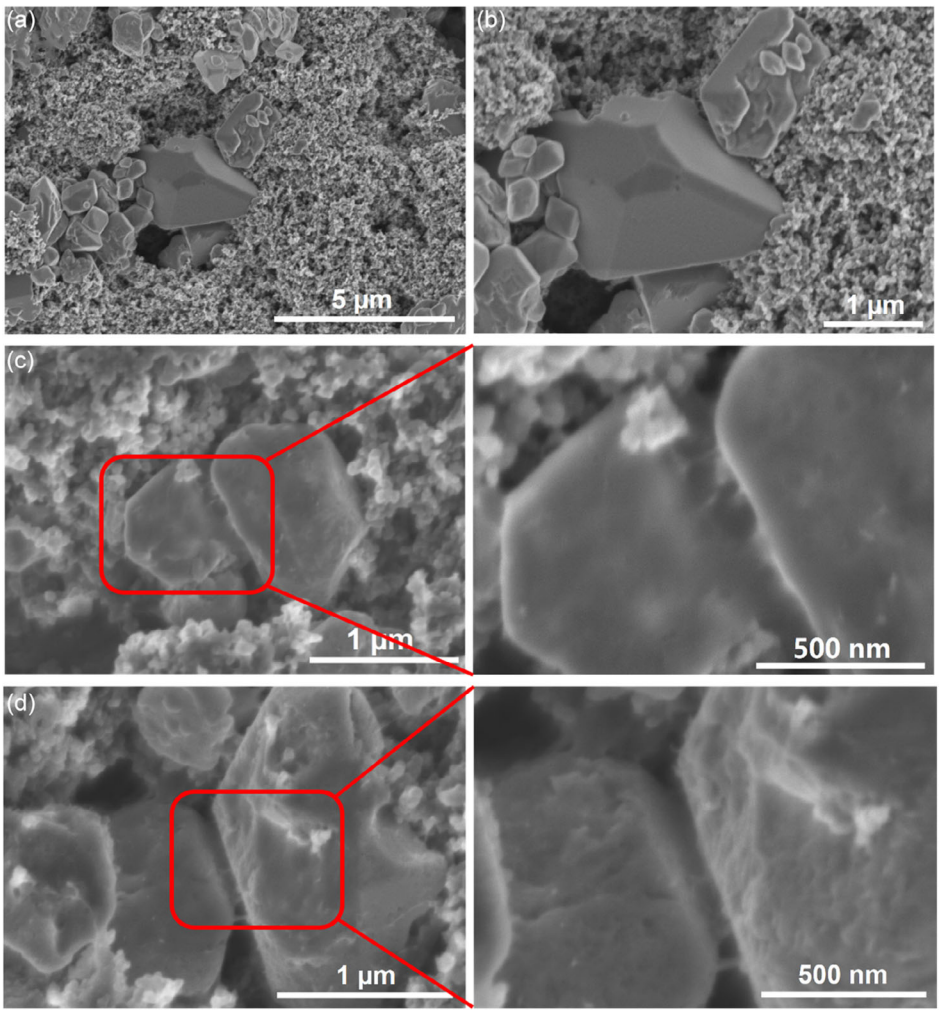

Figure 6. SEM images for TBDS electrodes a,b) before and c,d) after cycling.

10 cycles are provided in Figure S12, Supporting Information. An obvious XRD peak change can be observed after the 1st cycle, and the XRD peaks are well retained thereafter. These results demonstrate that the molecular structure of TBDS is retained, but its crystal structure is changed after initial cycles, which is coincident to the equilibrium potential change after the first discharge in the GITT result.

Since TBDS retains its molecular structure upon cycling, the hydrogen bonding between hydroxyl group and carbonyl group in TBDS is also retained. To verify the hydrogen bonding-induced self-healing chemistry, we further exploit the morphology change of TBDS before and after cycling. The cutoff window for the TBDS electrodes is from 1.5 V to 3.0 V versus Na/Na^+, and the electrolyte is 1 M $NaPF_6$ in DEGDME. The ether-based electrolyte is stable in this cutoff window, so the formation of the interphase by the decomposition of the electrolyte in the cycled TBDS electrodes is minimized. The impact of the interphase to intermolecular hydrogen bonding between TBDS molecules is minimal. The H–H interactions between the hydroxyl groups in TBDS enable the self-healing chemistry in the pulverized TBDS electrode to self-heal the cracks as shown in **Figure 6**. The healing of particle pulverization in the cycled TBDS electrode mitigates the degradation of the TBDS electrode in SIBs. Figure 6a,b shows the pristine TBDS electrode, consisting of intact TBDS micro-particles. After 5 cycles, obvious cracks can be observed in the cycled TBDS electrodes (Figure 6c,d). Though there are some cracks in the cycled electrode, apparent connection between the cracked particles still exists due to the hydrogen bonding between hydroxyl group and carbonyl group in TBDS. The cracked particles are still connected with each other, retaining the structure integrity of the micro-sized particles. This is a key indication of the self-healing chemistry. As indicated by our previous work, micro-sized organic particles suffer from severe particle pulverization due to large-volume expansion and shrinkage in the repeated charge and discharge processes.[11,29] This results in fast capacity loss of organic SIBs upon long-term cycling. There are three strategies to address this challenge: 1) reducing the organic particle size from microscale to nanoscale; 2) carbon coating; and 3) self-healing chemistry. We proved that design and synthesis of organic nanomaterials and carbon-coated organic materials can mitigate the particle pulverization at the price of lower volumetric capacity. In addition, the self-healing chemistry enabled by the self-healing polymer binder is also effective to mitigate the particle pulverization, but a large amount of binder (15 wt%) is required in the organic electrodes, lowering the capacity and energy density of organic SIBs. Therefore, we employed TBDS as the organic active material, leveraging intermolecular hydrogen bonding among hydroxyl groups in TBDS to enable the self-healing chemistry. TBDS exhibits higher capacity and cyclic stability than DBDS, which lacks hydroxyl groups to form intermolecular hydrogen bonding. The SEM results in Figure 6 confirm the intermolecular hydrogen bonding-enabled self-healing chemistry, which self-heals the pulverization in the TBDS electrodes. Therefore, the electrochemical behaviors and morphology change of TBDS upon cycling illustrate that the intermolecular hydrogen bonding-enabled self-healing chemistry is promising for developing high-stability and high-sustainability SIBs.

3. Conclusion

In summary, a self-healing organic material based on hydroxyl group and carbonyl group is reported for the high-stability and high-sustainability organic SIB cathode. The hydrogen bonding-enabled self-healing chemistry enables the superior electrochemical performance of TBDS, in terms of long cycle life (1000 cycles) and high-rate capability (up to 2 A g^{-1}). CV, GITT, and EIS techniques are used to exploit fast reaction kinetics. Na-ion diffusion-controlled reaction kinetics is observed with a very small overpotential after the first sodiation process, demonstrating fast Na-ion diffusion in TBDS. Ex situ/in situ FTIR, Raman, and XRD characterizations further prove the stable molecular structure of TBDS upon cycling. An obvious crystalline phase change is observed after the first sodiation process, but the newly formed crystalline structure is highly reversible in the following cycles, demonstrating good structural retention during the sodiation/desodiation process. The excellent structural stability is ascribed to the self-healing chemistry between hydroxyl group and carbonyl group in TBDS, which is confirmed by FTIR and SEM results. Therefore, the organic materials with intermolecular hydrogen bonding-enabled self-healing chemistry are promising for developing high-stability and high-sustainability SIBs.

Supporting Information

Supporting Information is available from the Wiley Online Library or from the author.

Acknowledgements

This work was supported by the US National Science Foundation Award No. 2000102. The authors also acknowledge the support from the Nanostructures for Electrical Energy Storage (NEES), an Energy Frontier Research Center funded by the US Department of Energy, Office of Science, Basic Energy Sciences, under Award number DESC0001160. Research at the Argonne National Laboratory was funded by the US Department of Energy (DOE), Vehicle Technologies Office. Support from Tien Duong of the US DOE's Office of Vehicle Technologies Program is gratefully acknowledged. Use of the Advanced Photon Source (APS), an Office of Science user facilities, was supported by the US Department of Energy, Office of Science and Office of Basic Energy Sciences, under contract no. DE-AC02-06CH11357.

Conflict of Interest

The authors declare no conflict of interest.

Data Availability Statement

The data that support the findings of this study are available from the corresponding author upon reasonable request.

Keywords

cathodes, hydrogen bonding, self-healing chemistry, sodium-ion batteries, tetrahydroxy-1,4-benzoquinone disodium salt

Received: June 15, 2023
Revised: August 4, 2023
Published online:

[1] V. Palomares, P. Serras, I. Villaluenga, K. B. Hueso, J. Carretero-González, T. Rojo, *Energy Environ. Sci.* **2012**, *5*, 5884.
[2] M. D. Slater, D. Kim, E. Lee, C. S. Johnson, *Adv. Funct. Mater.* **2013**, *23*, 947.
[3] H. Pan, Y. S. Hu, L. Chen, *Energy Environ. Sci.* **2013**, *6*, 2338.
[4] P. K. Nayak, L. Yang, W. Brehm, P. Adelhelm, *Angew. Chem. Int. Ed.* **2018**, *57*, 102.
[5] C. Delmas, *Adv. Energy Mater.* **2018**, *8*, 1703137.
[6] J. Deng, W. Bin Luo, S. L. Chou, H. K. Liu, S. X. Dou, *Adv. Energy Mater.* **2018**, *8*, 1701428.
[7] Y. Liu, Y. Xu, Y. Zhu, J. N. Culver, C. A. Lundgren, K. Xu, C. Wang, *ACS Nano* **2013**, *7*, 3627.
[8] J. Wang, C. Luo, T. Gao, A. Langrock, A. C. Mignerey, C. Wang, *Small* **2015**, *11*, 473.
[9] Z. Hu, L. Wang, K. Zhang, J. Wang, F. Cheng, Z. Tao, J. Chen, *Angew. Chem. Int. Ed.* **2014**, *53*, 12794.
[10] C. Luo, J. Wang, X. Fan, Y. Zhu, F. Han, L. Suo, C. Wang, *Nano Energy* **2015**, *13*, 537.
[11] C. Luo, Y. Zhu, Y. Xu, Y. Liu, T. Gao, J. Wang, C. Wang, *J. Power Sources* **2014**, *250*, 372.
[12] P. Commins, H. Hara, P. Naumov, *Angew. Chem. Int. Ed.* **2016**, *55*, 13028.
[13] D. Döhler, P. Michael, W. H. Binder, *Acc. Chem. Res.* **2017**, *50*, 2610.
[14] Y. K. Jeong, J. W. Choi, *ACS Nano* **2019**, *13*, 8364.
[15] Q. Li, D. G. Barrett, P. B. Messersmith, N. Holten-Andersen, *ACS Nano* **2016**, *10*, 1317.
[16] A. Vidyasagar, K. Handore, K. M. Sureshan, *Angew. Chem. Int. Ed.* **2011**, *50*, 8021.
[17] Z. Chen, C. Wang, J. Lopez, Z. Lu, Y. Cui, Z. Bao, *Adv. Energy Mater.* **2015**, *5*, 1401826.
[18] J. M. Whiteley, P. Taynton, W. Zhang, S. H. Lee, *Adv. Mater.* **2015**, *27*, 6922.
[19] Y. Zhao, Y. Zhang, H. Sun, X. Dong, J. Cao, L. Wang, Y. Xu, J. Ren, Y. Hwang, I. H. Son, X. Huang, Y. Wang, H. Peng, *Angew. Chem. Int. Ed.* **2016**, *55*, 14384.
[20] X. Fan, J. Mao, Y. Zhu, C. Luo, L. Suo, T. Gao, F. Han, S. C. Liou, C. Wang, *Adv. Energy Mater.* **2015**, *5*, 1500174.
[21] X. Y. Zhang, W. L. Song, Z. Liu, H. Sen Chen, T. Li, Y. Wei, D. N. Fang, *J. Mater. Chem. A* **2017**, *5*, 12793.
[22] R. Yi, F. Dai, M. L. Gordin, H. Sohn, D. Wang, *Adv. Energy Mater.* **2013**, *3*, 1507.
[23] J. Lee, J. Moon, S. A. Han, J. Kim, V. Malgras, Y. U. Heo, H. Kim, S. M. Lee, H. K. Liu, S. X. Dou, Y. Yamauchi, M. S. Park, J. H. Kim, *ACS Nano* **2019**, *13*, 9607.
[24] L. Zhang, C. Wang, Y. Dou, N. Cheng, D. Cui, Y. Du, P. Liu, M. Al-Mamun, S. Zhang, H. Zhao, *Angew. Chem. Int. Ed.* **2019**, *58*, 8824.
[25] Y. Yuan, W. Xiao, Z. Wang, D. J. Fray, X. Jin, *Angew. Chem. Int. Ed.* **2018**, *57*, 15743.
[26] H. Shang, Z. Zuo, L. Yu, F. Wang, F. He, Y. Li, *Adv. Mater.* **2018**, *30*, 1801459.
[27] J. I. Hur, L. C. Smith, B. Dunn, *Joule* **2018**, *2*, 1187.
[28] C. Wang, H. Wu, Z. Chen, M. T. Mcdowell, Y. Cui, Z. Bao, *Nat. Chem.* **2013**, *5*, 1042.
[29] C. Luo, X. Fan, Z. Ma, T. Gao, C. Wang, *Chem.* **2017**, *3*, 1050.
[30] T. B. Schon, B. T. McAllister, P. F. Li, D. S. Seferos, *Chem. Soc. Rev.* **2016**, *45*, 6345.
[31] Z. Song, H. Zhou, *Energy Environ. Sci.* **2013**, *6*, 2280.
[32] Q. Zhao, Y. Lu, J. Chen, *Adv. Energy Mater.* **2017**, *7*, 1601792.
[33] B. Häupler, A. Wild, U. S. Schubert, *Adv. Energy Mater.* **2015**, *5*, 1402034.
[34] Y. Liang, Z. Tao, J. Chen, *Adv. Energy Mater.* **2012**, *2*, 742.
[35] S. Muench, A. Wild, C. Friebe, B. Häupler, T. Janoschka, U. S. Schubert, *Chem. Rev.* **2016**, *116*, 9438.
[36] T. B. Schon, A. J. Tilley, C. R. Bridges, M. B. Miltenburg, D. S. Seferos, *Adv. Funct. Mater.* **2016**, *26*, 6896.
[37] Z. Luo, L. Liu, J. Ning, K. Lei, Y. Lu, F. Li, J. Chen, *Angew. Chem. Int. Ed.* **2018**, *57*, 9443.
[38] J. Xie, W. Chen, G. Long, W. Gao, Z. J. Xu, M. Liu, Q. Zhang, *J. Mater. Chem. A* **2018**, *6*, 12985.
[39] D. Chen, A. J. Avestro, Z. Chen, J. Sun, S. Wang, M. Xiao, Z. Erno, M. M. Algaradah, M. S. Nassar, K. Amine, Y. Meng, J. F. Stoddart, *Adv. Mater.* **2015**, *27*, 2907.
[40] S. Zheng, D. Shi, T. Sun, L. Zhang, W. Zhang, Y. Li, Z. Guo, Z. Tao, J. Chen, *Angew. Chem. Int. Ed.* **2023**, *62*, e202217710.
[41] M. Miroshnikov, K. Kato, G. Babu, N. Kumar, K. Mahankali, E. Hohenstein, H. Wang, S. Satapathy, K. P. Divya, H. Asare, L. M. R. Arava, P. M. Ajayan, G. John, *ACS Appl. Energy Mater.* **2019**, *2*, 8596.
[42] M. R. Tuttle, S. T. Davis, S. Zhang, *ACS Energy Lett.* **2021**, *6*, 643.
[43] H. Zhang, Y. Gao, M. Chen, L. Li, L. Li, Y. Qiao, W. Li, J. Wang, S. L. Chou, *Small Methods* **2022**, *6*, 2200455.
[44] M. Gorman, *J. Chem. Educ.* **1957**, *34*, 304.
[45] V. Augustyn, J. Come, M. A. Lowe, J. W. Kim, P. L. Taberna, S. H. Tolbert, H. D. Abruña, P. Simon, B. Dunn, *Nat. Mater.* **2013**, *12*, 518.